Earth and Planetary Science Letters 509 (2019) 38–46

Contents lists available at ScienceDirect

Earth and Planetary Science Letters

www.elsevier.com/locate/epsl

Archaeal ammonia oxidation plays a part in late Quaternary nitrogen cycling in the South China Sea

Liang Dong [a,b], Zhiyang Li [c], Guodong Jia [a,*]

[a] State Key Laboratory of Marine Geology, Tongji University, Shanghai 200092, China
[b] State Key Laboratory of Microbial Metabolism, School of Life Sciences and Biotechnology, Shanghai Jiao Tong University, Shanghai 200240, China
[c] Guangdong AIB Polytechnic College, Guangzhou 5510507, China

ARTICLE INFO

Article history:
Received 26 February 2018
Received in revised form 10 December 2018
Accepted 21 December 2018
Available online 8 January 2019
Editor: J. Adkins

Keywords:
ammonia oxidizing archaea
biomarker
nitrogen isotope
sediment records
late Quaternary

ABSTRACT

Thaumarchaeota, as an ammonia oxidizing archaea (AOA), is crucial for modern marine nitrogen cycling; however, little is known about its history during the Quaternary climate change. Here, isoprenoidal glycerol dialkyl glycerol tetraethers (GDGTs), biomarkers of *Thaumarchaeota*, were used to trace the role of AOA in the South China Sea (SCS) for the past 160 kyr. The GDGT-[2]/[3] ratio was firstly argued as an indicator of contribution of shallow *Thaumarchaeota* cluster that is more active in ammonia oxidization (AO) than the deep cluster, and then, was used to reconstruct AO in the past. The inferred AO exhibited intensification in the interglacials, and moreover, showed strong precessional cycles with enhancements at the precessional maxima when boreal winter insolation was the highest. The AOA record varied in line with isotope record of organic nitrogen ($\delta^{15}N_{org}$) that is modulated by the strength of diazotroph N_2 fixation (NF), suggesting a close coupling of increased AO with enhanced NF during periods of weak east Asian winter monsoon (EAWM) and hence increase of upper water stratification. AO intensification, a step of a series of dissolved oxygen consuming processes, is hereby hypothesized to encourage NF when the EAWM weakens. This result might be a reference for the future NF trend in the current situation of enhanced ocean deoxygenation due to global warming.

1. Introduction

In tropical oceans, nitrogen isotope ratio ($\delta^{15}N$) in sediments mainly reflect the balance in the history of N inputs from the atmosphere via N_2 fixation (NF) and N losses to the atmosphere via the anaerobic processes of denitrification and anaerobic ammonium oxidation (anammox) (Altabet et al., 1995; Higginson et al., 2003; Canfield et al., 2010; Mobius et al., 2011). $\delta^{15}N$ is powerful because NF introduces reactive N with little isotope discrimination ($\varepsilon \approx -1‰$; Wada and Hattori, 1976; Liu et al., 1996), whereas water column denitrification (WCD) preferentially removes ^{14}N-enriched nitrate (NO_3^-) with ε values up to 20–30‰ (Cline and Kaplan, 1975; Brandes et al., 1998; Altabet et al., 1999). Signal of past NF is evident or conjecturable in the oligotrophic western low latitude Atlantic and Pacific. For instance, several bulk $\delta^{15}N$ records in the western Pacific marginal seas generally show less significant glacial–interglacial changes (Kienast, 2000; Horikawa et al., 2006; Kao et al., 2008; Jia and Li, 2011). This pattern is in contrast to the $\delta^{15}N$ records from WCD areas such as the Arabian Sea and the East Tropical Pacific, exhibiting higher values in the interglacials indicating enhanced denitrification and lower values in the glacials indicating reduced denitrification (Altabet et al., 1995; Ganeshram et al., 1995). This likely resulted from the coupling of local NF with the regional denitrification signal transported from the east tropical Pacific, and thus, suggests an increased NF during the interglacials (Jia and Li, 2011). The $\delta^{15}N$ from planktonic foraminifera shells ($\delta^{15}N_{foram}$) is more specific than bulk $\delta^{15}N$ to infer thermocline nitrate $\delta^{15}N$, which clearly indicates an increased NF during the interglacials in the South China Sea (SCS), the Caribbean Sea, and the Gulf of Mexico (Ren et al., 2009, 2012, 2017; Meckler et al., 2011; Straub et al., 2013). However, the cause for NF variations is still in dispute, mostly focusing on the availability of iron (Falkowski, 1997; Broecker and Henderson, 1998; Moore et al., 2009) or phosphorus (Deutsch et al., 2007; Straub et al., 2013; Ren et al., 2017), which are the two main hypothesized limiting nutrients for marine NF. In modern oceans NF generally occurs in conditions with strong stratification, shallow mixed layers, and high solar energy fluxes (Luo et al., 2014; Benavides and Voss, 2015). A statistical analysis of global NF data indicates that solar radiation and subsurface minimum dissolved oxygen are the most influential factors determining diazotrophic

* Corresponding author.
E-mail address: jiagd@tongji.edu.cn (G. Jia).

https://doi.org/10.1016/j.epsl.2018.12.023
0012-821X/

activity, whereas P and dust-derived Fe do not appear to influence the spatial patterns of NF on global scale (Luo et al., 2014).

Besides, oceanic N cycling is far more complex than NF and denitrification as recorded by δ^{15}N. For example, there is a knowledge gap on nitrification in past climate cycles, a process that creates nitrate from released ammonia from organic matter (OM) degradation. Because nitrate is the primary form of nitrogen responsible for "new" production and the substrate for denitrification, nitrification is crucial for biological carbon pump and acts as a biogeochemical bridge between N inputs and N losses (Francis et al., 2007; Canfield et al., 2010). However, marine N cycling in the past is hard to trace by δ^{15}N method in oligotrophic waters due to complete N utilization that may not leave significant isotopic imprints of N processes except NF and denitrification. Therefore, in addition to δ^{15}N, proxies for specific N processes such as organic biomarkers (Rush and Sinninghe Damsté, 2017) are necessary to trace detailed oceanic N cycling.

Nitrification is fulfilled via two sequential steps, i.e., first ammonia oxidation (AO) and then nitrite oxidation. AO is usually the rate-limiting step of nitrification implemented by ammonia-oxidizing bacteria (AOB) (Koops and Pommerening-Roser, 2001) and archaea (AOA) (Spang et al., 2010). In marine environment, AOA are ubiquitous and dominant over AOB, with archaeal *amoA* gene abundance generally 1 to 2 orders of magnitude higher than bacterial *amoA* (Wuchter et al., 2006; Beman et al., 2008; Peng et al., 2015), and responsible primarily for AO (Peng et al., 2015). It has been widely recognized that the compound of crenarchaeol, an isoprenoid glycerol dialkyl glycerol tetraether (GDGT) containing one cyclohexyl moiety and four cyclopentyl moieties on its alkyl chain backbones, may be a specific biomarker of AOA or *Thaumarchaeota* (Spang et al., 2010; Stahl and de la Torre, 2012). So, crenarchaeol, as well as related GDGTs, may be an effective proxy for marine AO as well as nitrification. We believe that a combined use of δ^{15}N and GDGT records may advance the understanding of marine N cycling in addition to NF or denitrification. Here, we used this method by measuring sedimentary GDGTs and δ^{15}N in the last two glacial–interglacial cycles in the SCS. We will show that AOA may indeed have played a significant role in the paleo N cycles.

2. Materials and methods

2.1. Sediment cores and age model

A sediment core MD05-2897 (08°49.53′N, 111°26.51′E; water depth 1658 m; core length 30.98 m) located in the southern SCS were studied in this work (Fig. 1). The age model of the core was established by Huang and Tian (2012) based on both the isotopic aligning and a set of planktonic foraminiferal ^{14}C measurements. In detail, its upper part was constrained by a set of planktonic foraminiferal ^{14}C ages, while its lower part was established through tuning the planktonic foraminiferal δ^{18}O to Chinese stalagmite δ^{18}O records (Wang et al., 2008) and tuning the benthic foraminiferal δ^{18}O record to the global benthic δ^{18}O stack LR04 (Lisiecki and Raymo, 2005). Unfortunately, this core covers a history from 22 ka to 175 ka with the younger part lost during sampling. In order to make up the lost part, the upper 6.80 m of core MD01-2392 (09°51.13′N, 110°12.64′E; water depth 1966 m; Fig. 1) in the same area was utilized, representing the last 26 kyr. The age model of MD01-2392 was established by Li et al. (2010) through comparing the foraminiferal oxygen isotope with the published curves, especially the global δ^{18}O stack of Lisiecki and Raymo (2005) and results from ODP site 1143 (Tian et al., 2004). Therefore, we were able to integrate the two cores into a continuous sequence covering the last two glacial–interglacial cycles, from the marine isotope stage (MIS) 6 to the MIS 1.

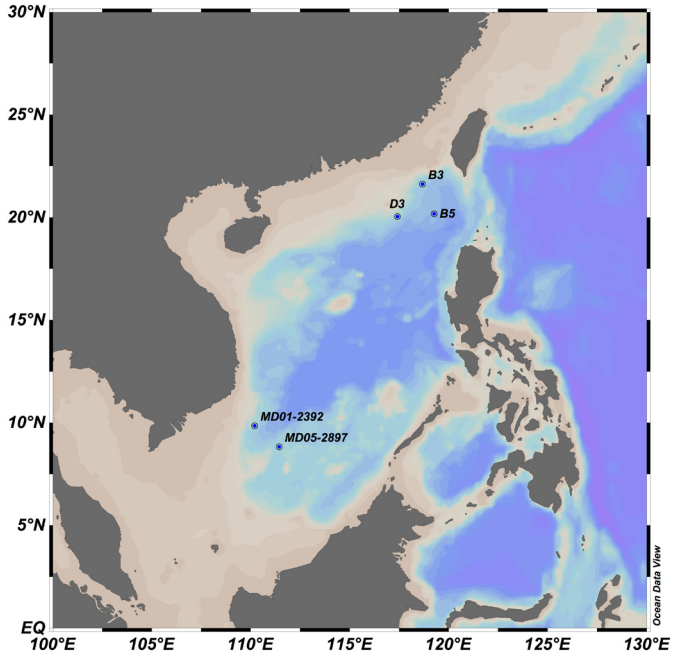

Fig. 1. Study sites in the SCS. Sites B3, B5 and D3 are for suspended particulate matter in water columns and sites MD01-2392 and MD05-2897 for two sediment cores.

Additionally, suspended particulate matters (SPM) in the water column of the SCS were also collected at three stations (Fig. 1) for GDGT analysis in support of interpretation of sedimentary data. These SPM were filtered over 500 L waters at different water depths (100 m, 300 m, 1000 m, 2000 m) in spring, 2013 on pre-combusted (at 450 °C) glass fiber filters (GF/F, 0.7 μm, 142 mm diameter, Whatman) using an in-situ bulk filter system. Because of extremely low GDGT concentration in surface water, a larger volume of surface water near the D3 station was additionally collected.

2.2. Lipid extraction and analysis

Freeze-dried sediment and SPM samples were extracted ultrasonically using dichloromethane (DCM)/MeOH (3:1, V/V) for four times after addition of a C_{46} tetraether as an internal standard. For each total lipid extract, an aliquot was concentrated, and then filtered through a 0.45 μm PTFE filter before HPLC analysis.

Analyses of GDGTs were performed at Tongji University by a slightly modified method of Schouten et al. (2002). Separation was achieved using an Agilent 1200 liquid chromatograph equipped with an automatic injector and a Prevail Cyano column (2.1 by 150 mm, 3 μm; Alltech, Deerfield, IL), maintained at 40 °C. GDGTs were firstly eluted isocratically with *n*-hexane and isopropanol as follows: 99% *n*-hexane and 1% isopropanol for 5 min and then a linear gradient to 1.8% isopropanol in 45 min. The flow rate was 0.2 ml/min. After each analysis, the column was cleaned by back flushing with *n*-hexane-isopropanol (90:10, V/V) at 0.2 ml/min for 10 min. Detection was performed using an Agilent 6460 triple-quadrupole mass spectrometer (MS) with an atmospheric pressure chemical ionization (APCI) ion source. Conditions for APCI MS were as follows: nebulizer pressure, 60 lb/in^2; vaporizer temperature, 400 °C; drying gas (N_2) flow, 5 l/min; temperature, 200 °C; capillary voltage, −3.5 kV; corona, 5 μA (3.2 kV). The single-ion monitoring (SIM) mode was used to detect the eight isoprenoidal and branched GDGTs (m/z 1302, 1300, 1298, 1296, 1292, 1050, 1036, and 1022) and the C_{46} internal standard (m/z 744), with a dwell time of 237 ms per ion.

2.3. Sample treatment for isotope analysis

Inorganic N trapped in clay minerals is a significant part of total N in the SCS (Kienast et al., 2005), which may discount the application of $\delta^{15}N_{total}$ to accurately reflect upper water $\delta^{15}N_{org}$, and in turn nitrate $\delta^{15}N$. To eliminate this interference, a method introduce by Li and Jia (2011) was used in this study. Briefly, freeze-dried sediments were digested with 1 M HCl to remove carbonate and then with 5 M HF/1 M HCl to remove clay minerals. The final dark solid residue was mainly organic. Trace amounts of OM dissolved in the HCl and HF–HCl solutions were recovered by solid phase extraction (0.5 g PPL cartridge, Varian) according to the procedure described by Dittmar et al. (2008) and combined with the solid residue to obtain total OM. The obtained total OM was thoroughly freeze-dried and homogenized before isotope analysis.

Isotope analysis of OM was performed using an isotope ratio mass spectrometer (DELTA^{plus}XL) interfaced with a C/N/S analyzer (CE EA1112). Carbon and nitrogen isotope ratios are expressed in conventional delta (δ) notation, which is the per mil (‰) deviation from the standard of Pee Dee Belemnite (PDB) and air N_2, respectively, with precisions of ±0.2‰ for $\delta^{13}C$ and ±0.3‰ for $\delta^{15}N$.

3. Results

3.1. GDGT results in SPM and sediments

Crenarchaeol (Cren) was the most abundant compound among the six common isoprenoid GDGTs in SPM, with GDGT-0 (here short as [0], the compound not containing cyclic ring) the second most and the [0]/cren ratio in the range of 0.22–0.48 (Fig. 2). Cren correlated significantly with the other individual isoprenoid GDGTs ($r^2 > 0.95$, $p < 0.01$). Cren concentration in the SPM at the three stations showed consistently highest values between 18.1 and 20.4 ng/l at the water depth of 100 m. And then, it exhibited a decreasing trend downward to 2000 m, with the fastest decease from 100 to 300 m and nearly constant between 1000 to 2000 m depth (Fig. 2). In the surface water at the D3 station cren concentration was much lower, only 0.027 ng/l, than in deeper waters at the three stations. The ratio of GDGT-2 to GDGT-3 (here short as [2]/[3]), the compounds containing two and three pentacyclic rings, respectively, exhibited lower values in surface water (~1.2) and at the 100 m depth (2.8–3.5) and rose to higher values (mostly between 5.9–8.6) below 300 m depth (Fig. 2).

Similar to the GDGT composition in the SPM, in downcore sediments cren and GDGT-0 was also the two most abundant compounds, with [0]/cren ratio in the range of 0.26–0.53. Also, cren correlated well with other individual GDGTs (Fig. 3). The concentration of cren in core MD05-2897 varied between 14.5 ng/g and 476.9 ng/g (Fig. 4d). It exhibited roughly slight increases during warm periods, i.e., MISs 3 and 5, relative to the cold periods, i.e., MISs 4 and 6. In core MD01-2392, this pattern persisted, showing the lowest values between 32.6 ng/g and 523.3 ng/g with an average of 147.4 ng/g during MIS 2, but then increased moderately to a range between 11.3 ng/g and 643.1 ng/g with an average of 310.3 ng/g in the Holocene (Fig. 4d).

The [2]/[3] ratio downcore MD05-2897 (Fig. 4e) showed a clear glacial–interglacial variation from MIS 6 to MIS 3, with lower values (6.80 ± 0.53) occurring between MIS 5 and early MIS 4 and higher values during MIS 6 (8.07 ± 0.33) and between late MIS 4 and MIS 3 (8.0 ± 0.52). Down the core MD01-2392, the [2]/[3] ratio exhibited a similar pattern with higher values (9.03 ± 1.21) during MIS 2, and lower values (7.78 ± 1.21) during MIS 1. Fluctuations of [2]/[3] record displayed a strong precessional cycles (Fig. 4e1). Besides, lowerer [2]/[3] ratios largely corresponded to higher cren concentrations.

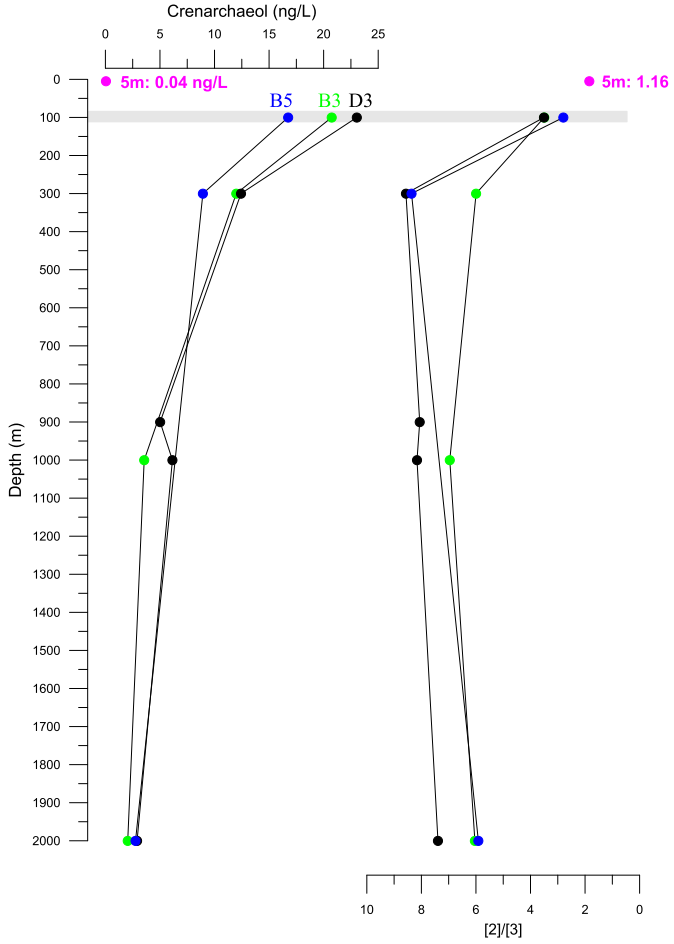

Fig. 2. Profiles of cren concentration and GDGT-[2]/[3] ratio of suspended particles in the water column. (For interpretation of the colors in the figure(s), the reader is referred to the web version of this article.)

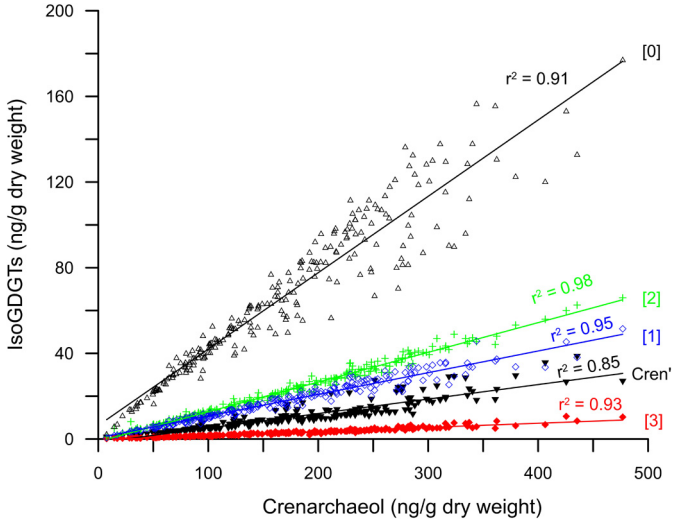

Fig. 3. Scatter plot showing relationship of cren with other isoprenoid GDGTs. The symbol of [0] denotes GDGT containing zero cyclopentyl moieties on its alkyl chain backbones, and so on. Cren' is the crenarchaeol isomer.

3.2. Organic $\delta^{15}N$ records

The $\delta^{13}C_{org}$ values down the two cores were similar in range and varied narrowly between −19.8‰ and −22.1‰ (data not shown). The $\delta^{15}N_{org}$ showed higher values during the glacials and

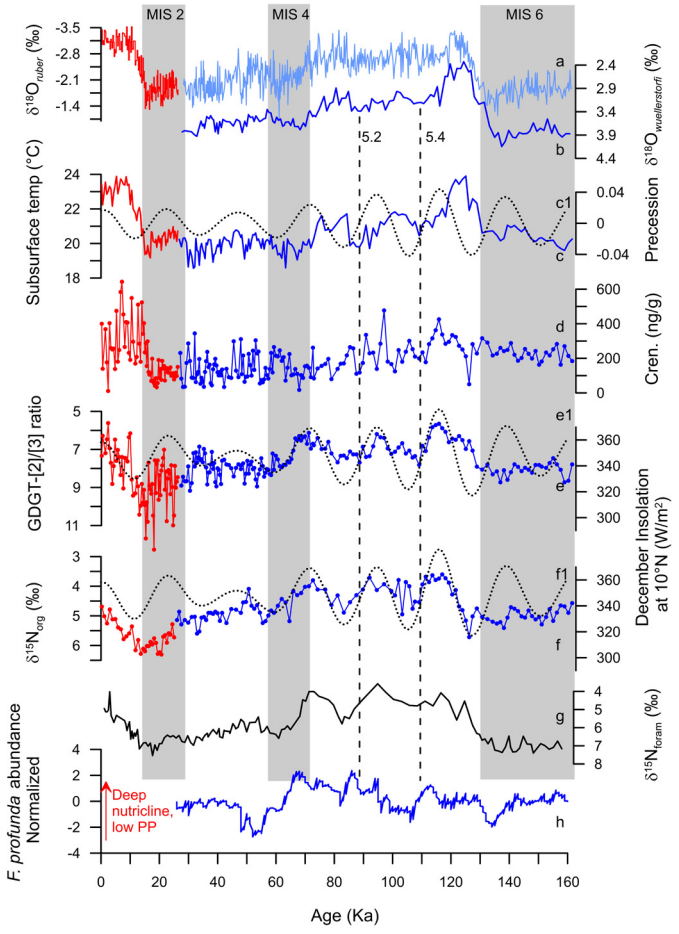

Fig. 4. Combined records of MD01-2392 (red) and MD05-2897 (blue) from Marine Isotope Stage (MIS) 6 to 1. (a) Planktonic foraminifer *Globigerinoides ruber* δ^{18}O; (b) Benthic foraminifer *Cibicidoides wuellerstorfi* δ^{18}O; (c) TEX_{86}^{H}-derived subsurface temperature (Dong et al., 2015); (c1) Precession cycles (d) Crenarchaeol content; (e) GDGT-[2]/[3] ratio and (e1) December insolation at 10°N; (f) δ^{15}N of organic matter and (f1) December insolation at 10°N; (g) Planktonic foraminifer δ^{15}N from site MD97-2142 in the southeastern SCS (Ren et al., 2017); (f) Normalized abundance of coccolithophore *Florisphaera profunda* reflective of nutricline dynamics downcore MD05-2897 (Su et al., 2013).

lower values during the interglacials (Fig. 4f). For example, $\delta^{15}N_{org}$ ranged between 4.5‰ and 5.5‰ during MIS 6 and between 4.9‰ and 6.3‰ during MIS 2, whereas it varied mostly between 3.5‰ and 5.0‰ during MIS 5, and 4.5‰ and 6.0‰ during MIS 1 (Fig. 4f). In addition, $\delta^{15}N_{org}$ record also exhibited strong precessional cycles (Fig. 4f1) similar to the curve of GDGT [2]/[3]. Note that there were slight offsets in data values between the two cores and that the bulk δ^{15}N in the core MD01-2392, showing almost no glacial/interglacial change, have been reported elsewhere (Jia and Li, 2011).

4. Discussion

4.1. GDGT-[2]/[3] as an indicator of Thaumarchaeota community

Two major marine groups (MG) of planktonic archaea, i.e., MG I *Thaumarchaeota* and MG II *Euryarchaeota* are frequently found in oceans based on their 16S rRNA gene sequences (DeLong, 1992; Fuhrman et al., 1992). Typically, MG II *Euryarchaeota* are more abundant in epipelagic waters whereas MG I *Thaumarchaeota* are more productive below the photic zone (Massana et al., 2000; Karner et al., 2001; Herndl et al., 2005). A third archaeal group, MG III *Euryarchaeota*, have been also identified in deep seas (Fuhrman and Davis, 1997; Massana et al., 2000; Galand et al., 2009). In the SCS, MG II *Euryarchaeota* decrease in abundance from 87.7% to 0.4% at depths from 10 to 3000 m, whereas MG III *Euryarchaeota* increase from 9.2% to 57.4% (Tseng et al., 2015). Coincidently, MG I *Thaumarchaeota* are scarce in surface waters, then increase with depth to their maximum near the base of the euphotic zone or in the mesopelagic zone (50–200 m) and decrease again in the bathypelagic zone (Hu et al., 2011; Tseng et al., 2015). This distribution pattern occurs similarly in open oceans (Karner et al., 2001; Mincer et al., 2007; Church et al., 2010). Comparatively, the profiles of cren concentration in the SCS water column in this study mirrored the depth distribution of *Thaumarchaeota* abundance and are different from those of MG II and III *Euryarchaeota*, supportive of the thaumarchaeal origin of cren (Sinninghe Damsté et al., 2002). In addition, the narrow range of [0]/cren ratio here (i.e., 0.22–0.48) suggests a simple source for GDGTs (Turich et al., 2007), and the high correlations between cren and other GDGTs may demonstrate the same source for these GDGTs. Although a recent study suggests that *Euryarchaeota* are also capable of producing cren (Lincoln et al., 2014), it is yet to be identified because no pure cultures or even enrichments are available for *Euryarchaeota* (Zhang et al., 2015). So GDGTs are tentatively considered to be sourced from *Thaumarchaeota* in this study. That the maximum abundance of MG I *Thaumarchaeota* and associated GDGTs occur near the base of euphotic zone supports the GDGT-derived TEX_{86} proxy as an applicable indicator for subsurface temperature centering around 75 m depth in the SCS (Jia et al., 2012). Until now, this is still a debatable issue (Tierney and Tingley, 2015; Ho and Laepple, 2016; Zhang and Liu, 2018). Nevertheless, the linkage between GDGTs-derived proxy and the corresponding thermal signal is likely via the maximum primary productivity (PP) at the similar depth, which could support zooplankton grazing, thereby providing a potential mechanism for delivery of subsurface GDGT lipids to the sediments (Wuchter et al., 2005; Jia et al., 2012).

In addition to the vertical change of abundance, there occurs a shift of *Thaumarchaeota* community structure from a "shallow cluster" in the epipelagic layer to a "deep cluster" in the meso- and bathypelagic zones in the SCS (Hu et al., 2011; Xia et al., 2015; Tseng et al., 2015) and other seas (Mincer et al., 2007; Beman et al., 2008; Tolar et al., 2013; Villanueva et al., 2015). Correspondingly, analysis of intact polar lipid (IPL) of GDGTs, which is more closely associated with the living cells due to their relatively rapid turnover time, in marine water columns clearly shows different values of the [2]/[3] ratio between shallow water (1.2–3.3; 0–50 m depth) and deep water (4.0–21.5; 200–2431 m depth) in the Arabian Sea and along the Portuguese continental margin (Schouten et al., 2012; Kim et al., 2016). Therefore, high [2]/[3] ratio has been attributed to *Thaumarchaeota* thriving in deep waters (Schouten et al., 2012; Taylor et al., 2013; Kim et al., 2015, 2016). The reason for the different GDGT distributions between shallow and deep *Thaumarchaeota* remains unclear but might be associated with combined factors such as low oxygen, high pressure and nutrients (e.g., Basse et al., 2014; Villanueva et al., 2015). GDGT composition in SPM has been found to change regularly in numerous investigations, showing an increase of the [2]/[3] ratio with depth (Schouten et al., 2012; Taylor et al., 2013; Hernández-Sánchez et al., 2014; Kim et al., 2015, 2016). The profiles of the [2]/[3] ratio in the water column SPM in this study are consistent with those observations, showing lower values at depths of 0 and 100 m (<3.5) and higher values below 300 m (5.9–8.6). However, GDGTs analyzed here were core lipids that are not wholly produced in situ but composed of lipids from both fossil and living *Thaumarchaeota*, which may admix GDGTs from different depths, e.g., admixing of shallow thaumarchaeal GDGTs into deep ones in the course of particle sinking. Accordingly, the [2]/[3] ratio in SPM here may reflect relative contributions of shallow versus deep *Thaumarchaeota*. However, the [2]/[3] values in the living cell membranes of the two end

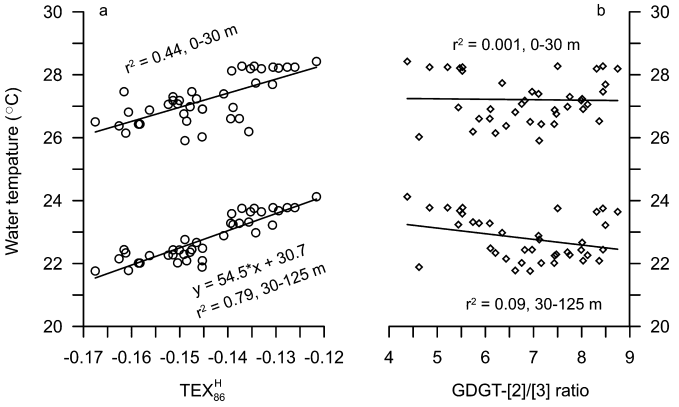

Fig. 5. Relationship of surface (0–30 m) and subsurface (30–125) water temperatures with (a) the TEX_{86}^H proxy and (b) the ratio of GDGT-[2]/[3] in core top sediments in the SCS. GDGT data are from Jia et al. (2012).

members are poorly constrained at present. Using the IPL-derived mean [2]/[3] ratio values of 2.5 and 13.5 in seawater column SPM for shallow and deep *Thaumarchaeota* (Schouten et al., 2012; Kim et al., 2016), respectively, our results suggest that shallow *Thaumarchaeota* could account for >90% GDGTs at 100 m depth and 57% (45%–69%) GDGTs for deeper waters. For comparison, using a similar method Jia et al. (2017) estimate that shallow *Thaumarchaeota* may contribute 61 ± 10% GDGTs in surface sediments in the open SCS. Such a significant contribution of shallow thaumarchaeal GDGTs to deep waters and sediments could be associated with the highest abundance of shallow *Thaumarchaeota* and their GDGTs occurring near the base of euphotic zone, where PP is high and OM may be downward exported efficiently. Need to mention that our study water columns were in the northern SCS whereas sediment cores were in the south. We consider this is not a serious problem because horizontally the archaeal populations, especially the *Thaumarchaeota*, show homogeneous distribution in the SCS (Hu et al., 2011).

In our downcore records, the cren abundance since MIS 6 was largely in parallel with the [2]/[3] curve, with higher cren contents roughly corresponding to lower [2]/[3] values (Fig. 4d, e). Some mismatches between them might be due to that cren content in sediments could be confounded by factors such as variations in degradation and sedimentation rate. The overall inverse correspondence between cren content and [2]/[3] ratio suggests that changes in the shallow *Thaumarchaeota* but not the deep ones should have determined variations in composition and content of thaumarchaeal GDGTs in sediments. The influence of shallow *Thaumarchaeota* on sedimentary GDGTs could be also implied by the fact that the TEX_{86} proxy in surface sediments correlates best with seawater temperature at ~75 m or 30–125 m depths in the open SCS (Fig. 5a; Jia et al., 2012), although deep *Thaumarchaeota* may contribute nearly half of sedimentary GDGTs (Jia et al., 2017). These occurrences suggest that the input to sedimentary lipids from deep *Thaumarchaeota* is relatively invariant, which needs to be justified in future. This conjecture is likely applicable to the past for a specific site, even if deep thaumarchaeal lipids might contribute more to deeper sites (Kim et al., 2016; Jia et al., 2017). We hereby preferred applying the [2]/[3] ratio, which would be less affected by degradation and sedimentation rate, rather than using cren content as the indicator of *Thaumarchaeota* community or the paleo productivity of shallow cluster in this study.

4.2. Changes of AO inferred from [2]/[3] record

Our downcore [2]/[3] record showed a general glacial–interglacial contrast with lower values suggestive of more shallow cluster *Thaumarchaeota* during the interglacials when the East Asian winter monsoon (EAWM) are greatly reduced. More intriguingly, lower values in the [2]/[3] variations were highly coherent and roughly in phase with the precession maxima when northern hemisphere experiences the warmest winters within the precession cycles (Fig. 4e and e1). The EAWM has been found to vary similarly in response to precession (Yamamoto et al., 2013). So, higher abundances of shallow *Thaumarchaeota* likely were correlated with weaker EAWM that could develop favorable environmental conditions for the ecotype. Several environmental factors such as temperature, light, ammonia availability and competition with phytoplankton have been suggested to influence *Thaumarchaeota* abundance and activity, especially for coastal shallow waters (Murray et al., 1998; Herfort et al., 2007; Urakawa et al., 2014; Liu et al., 2018). Weak EAWM would be conductive to warm sea temperatures beneficial for the shallow *Thaumarchaeota* (Qin et al., 2014; Schaefer and Hollibaugh, 2017; Liu et al., 2018). However, comparison of the [2]/[3] record with TEX_{86}-derived subsurface temperature indicates that [2]/[3] ratio did not track the TEX_{86} temperature, with the latter rose earlier than the precession maxima (Fig. 4c and c1). Hence, temperature change does not seem to directly control the shallow *Thaumarchaeota* abundance reconstructed from the [2]/[3] ratio.

However, the above inconsistency between the [2]/[3] and TEX_{86} records remind us to address that if the ratio of [2]/[3] is temperature dependent or not, which is risky as the relative distribution of cyclopentane rings in the GDGTs strongly depends on growing temperatures that leads to the development of TEX_{86} temperature proxy (Schouten et al., 2002). Recently, Taylor et al. (2013) elaborated on this issue and observed a weak but statistically significant positive correlation of [2]/[3] to SST in the modern core-top dataset of Kim et al. (2010). The authors thought that the relation behaves in the opposite manner to that expected based on the principle of homeoviscous adaptation (Shimada et al., 2002; Wuchter et al., 2004; Schouten et al., 2007; Pearson et al., 2008). Meanwhile, the authors found that sedimentary [2]/[3] ratio is also positively correlated with the overlying water depth and thereby proposed that water depth could influence the ratio by modulating relative contribution of shallow and deep ecotypes of *Thaumarchaeota* (Taylor et al., 2013). Here, our reanalysis of surface sedimentary GDGT data of Jia et al. (2012) did not show significant correlation between the [2]/[3] ratio and surface or subsurface water temperatures (Fig. 5b), in contrast to the TEX_{86} proxy that is highly correlated with subsurface temperature (Fig. 5a). Accordingly, we further deem that the use of [2]/[3] ratio as an indicator of *Thaumarchaeota* community or the paleo productivity of shallow *Thaumarchaeota* is applicable.

Come back to the influence of EAWM on shallow *Thaumarchaeota*, it actually may also change upper water conditions via wind strength, and profoundly contribute to PP by regulating the depth of nutricline in the SCS (Su et al., 2013, 2015). The relative abundance of coccolithophore *Florisphaera profunda* reflective of nutricline dynamics and PP down the core MD05-2897 shows strong precessional variations, with deep nutricline and hence low PP occurring during weak EAWM periods (Fig. 4h; Su et al., 2013), just when shallow *Thaumarchaeota* increased. The shallow *Thaumarchaeota* can actively perform oxidation of ammonia that is regenerated primarily from OM remineralization in the nutricline, with its maximum abundance following closely the depth of nutricline (Beman et al., 2012). In spite of not entirely overlapping in space between them, phytoplankton have been observed to compete with *Thaumarchaeota* for ammonia in the euphotic zone in both coastal waters (e.g., Murray et al., 1998; Herfort et al., 2007) and the open Pacific Ocean (Beman et al., 2012). We surmise the competitive mechanism could be applicable to the findings here as well, i.e., deep nutricline slows down

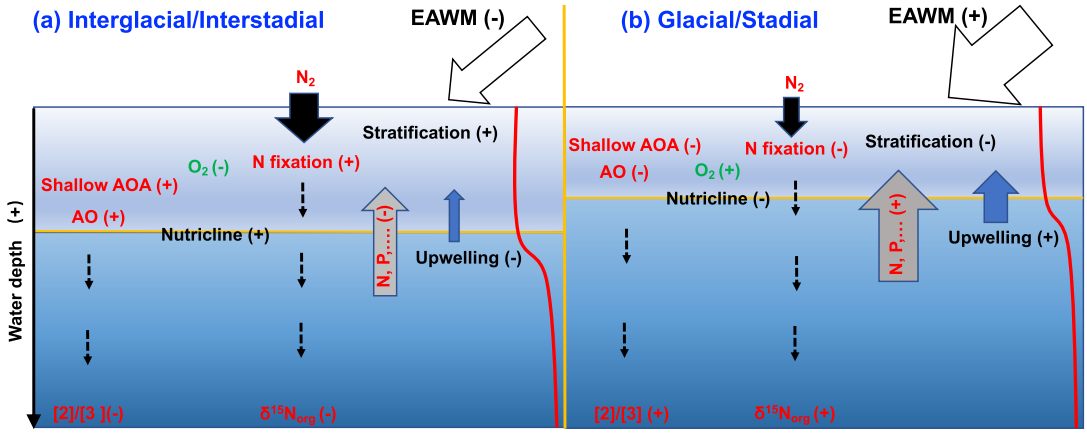

Fig. 6. Schematic figure of upper water nitrogen cycling in (a) the interglacial/interstadial vs. (b) the glacial/stadial.

the upward diffusion of regenerated ammonia and other nutrients, decreases PP, and leads to encouragement of *Thaumarchaeota* in the nutricline as well as in the euphotic zone.

The two phylogenetically different water column clusters of *Thaumarchaeota* are likely attributed to their adaptabilities to ammonia concentration, with the shallow cluster dominating in relatively high ammonia concentration environments and the deep cluster dominating in deep-ocean environments with ammonia concentrations below the detection limit of conventional methods (Sintes et al., 2013). In addition, they appear to differ in their abilities to oxidize ammonia. In the Gulf of California (Beman et al., 2008, 2012) and Monterey Bay (Smith et al., 2014) and along a 7500 km transect from the equatorial Pacific Ocean to the Arctic Ocean (Shiozaki et al., 2016), shallow AOA are reported to be responsible for the measured AO rate and the contribution from deep AOA is little. Therefore, our records observed here could reflect enhanced AO, likely as well as nitrification, in response to reduced upwelling, deepened nutricline and decreased PP due to the weakened EAWM during the precession maxima as illustrated in Fig. 6.

4.3. Coupling of AO and NF

In the SCS, $\delta^{15}N$ in bulk sediments shows less variation during glacial–interglacial cycles (Kienast, 2000; Jia and Li, 2011). Our $\delta^{15}N_{org}$ record here is presumably better than the bulk records to reflect nitrate $\delta^{15}N$ utilized by PP because our method removed interference of inorganic nitrogen. Besides, the $\delta^{13}C_{org}$ values between $-19.8‰$ and $-22.1‰$ are typical of marine derived OM, excluding the influence of terrestrial OM (Kienast et al., 2001). $\delta^{15}N_{org}$ values of 5.3–6.3‰ during MIS 2 are similar to the value of 5.6‰ of nitrate in the thermocline of the SCS during the last glacial estimated by using the $\delta^{15}N_{foram}$ data (Ren et al., 2012). According to the $\delta^{15}N_{foram}$ record, nitrate in the thermocline started to be ^{15}N depleted due to enhanced NF since the last deglaciation, and nitrate $\delta^{15}N$ decreased to ~4.4‰ in the late Holocene (Ren et al., 2012). Our $\delta^{15}N_{org}$ record is consistent with this variation pattern and showed $\delta^{15}N_{org}$ values ~5‰ in the late Holocene (Fig. 4f). More recently, a longer, 860-kyr record of $\delta^{15}N_{foram}$ is reported in the SCS (Ren et al., 2017). We found a close resemblance between our $\delta^{15}N_{org}$ record and the $\delta^{15}N_{foram}$ record for the past 160 kyr (Fig. 4f and g). Based on the reasoning by Ren et al. (2017), the glacial–interglacial variations in $\delta^{15}N_{foram}$ is controlled by NF that responses to glacial cycles in benthic N loss along the continental margins due to sea level change. However, both the $\delta^{15}N_{org}$ and $\delta^{15}N_{foram}$ records show strong variability at precession cycle during the past 160 kyr, exhibiting low $\delta^{15}N$ values at precession maxima (Fig. 4f and g). Such a prominent precession signal suggests that NF could be also regulated by insolation changes at low-latitudes, with the enhancement of NF when nutricline deepens during the precession maxima. This occurrence is consistent with modern observations that thermally stratified water is favorable for N_2 fixers (e.g., Church et al., 2009; Zehr and Kudela, 2011; Luo et al., 2014); however, it is not consistent with the opinions that, for example, the availability of iron (Falkowski, 1997; Broecker and Henderson, 1998; Moore et al., 2009) and/or phosphorus (Deutsch et al., 2007; Straub et al., 2013; Ren et al., 2017) would determine NF. In the SCS, both upwelling of N-depleted, phosphorus-bearing water in the deep thermocline (Wong et al., 2007; Ren et al., 2017) and dust-derived iron carried by strong EAWM have been suggested to promote NF (Wong et al., 2002; Wu et al., 2003). The latter, however, is not supported by sediment records showing reduced NF during the glacials when the EAWM was stronger (Ren et al., 2012, 2017). Based on our records, however, both the two elements of P and Fe are unlikely pivotal to NF in the paleo SCS, as the coincident weak EAWM and hence intensified water stratification would reduce northerly dust input and impede vertical mixing/upwelling, respectively.

The close resemblance of the GDGTs-[2]/[3] record to the $\delta^{15}N_{org}$ record (Fig. 4e and f) has never been found before. As shown above, the connection between them could be the physical dynamics in the upper water column induced by precessional insolation. The inferred covariation of AO and NF does not necessarily mean a causal relationship, especially considering the depth segregation between them, i.e., the maximum AO in the nutricline (Beman et al., 2012) whereas NF mainly in the nutrient-depleted layer above the nutricline (Du et al., 2017). In a recent study, however, surface solar radiation and subsurface minimum O_2 are identified to explain the most spatial variance in the observed NF data, whereas phosphorus and dust-derived iron are mute for the NF variance (Luo et al., 2014). The study shows that marine pelagic NF is high in the regions with high solar radiation and low subsurface dissolved O_2 beyond the areas of water column denitrification (Luo et al., 2014). Interestingly, enhanced NF is also closely connected with photic zone deoxygenation, water stratification and global warming in the geological deep times, e.g., across the Permian–Triassic boundary (Xie, 2018) and during the Cretaceous oceanic anoxic events (e.g., Kuypers et al., 2004), although biogeochemistry and paleoceanography were vastly different than Quaternary marine basins. We believe this occurrence could be associated with the fact that the activity of nitrogenase, the only microbial enzyme known to convert the N_2 molecule into ammonia, is dependent on the absence of O_2 (Berges and Mulholland, 2008). We accordingly surmise that O_2 depletion in epipelagic waters might be a mechanical connection between AO and NF for the coupling of records between GDGT [2]/[3] ratio and $\delta^{15}N_{org}$ observed here. This is because that microbial oxidizing of ammonia,

as well as its previous step of ammonia release from OM remineralization and subsequent step of nitrite oxidation, consumes O_2 from the environment (Zehr and Kudela, 2011). Thereby, elevated AO and associated processes would lower dissolved O_2 and potentially encourage NF, although the detailed controlling processes is unclear at present (Luo et al., 2014).

4.4. Implications

In addition to NF, we think that AOA may also have contributed to the lowering of euphotic nitrate $\delta^{15}N$ by release of the byproduct of N_2O during AO (Naqvi, 1991; Codispoti et al., 2001), because the $\delta^{15}N$ of N_2O produced by AOA is +6.2‰ versus supplied ammonia (Santoro et al., 2011). More production of N_2O due to enhanced AO during the interglacials is also consistent with elevated N_2O concentration in the atmosphere (Sowers et al., 2003). However, because of coupling between AO and NF in this study, the contribution of AO to the lowering of nitrate $\delta^{15}N$ is hard to be assessed here. Moreover, the N_2O yield by AOA is unknown at present, and it appears that only about 0.1 percent of ammonium is converted to N_2O by AOB (Cohen and Gordon, 1979), unlikely strong enough to compare with the isotope effect of NF.

According to Yool et al. (2007), globally 25–30% of all marine PP is sustained by nitrate that is produced by nitrification in the euphotic zone (EZN), suggesting that estimates of export production based on the f-ratio according to nitrate uptake rate (Eppley and Peterson, 1979) were significantly lower when accounting for EZN. During the periods of weak EAWM winds in glacial cycles and precessional cycles, AO, and likely EZN as well, would have been elevated based on our records. This means that PP during these periods, although declined, was supported by an increased fraction of regenerated N within the euphotic zone, thereby helping to lower the export production and weakening the biological carbon pump. In addition, O_2 consumption in the course of AO and associated processes, i.e. OM remineralization and nitrite oxidation, may contribute to O_2 depletion in epipelagic waters. Current global warming is leading to enhanced stratification, declined PP and O_2 depletion in the oceans (Polovina et al., 2008; Stramma et al., 2008; Boyce et al., 2010), likely similar to the scenario of weak EAWM wind-induced upper water stratification in this study. Since the trend and consequences of oceanic environments under current global warming are hard to predict, it is necessary in future works to explore the detailed biogeochemical and biological responses to the enhancement of upper water column stratification in the past.

5. Conclusions

The biomarker ratio of GDGT-[2]/[3] was applied to reconstruct marine thaumarchaeal community structure in terms of shallow versus deep clusters during the last two glacial–interglacial cycles in the SCS. The shallow cluster that is more active in oxidizing ammonia increased during the interglacials and precession maxima due likely to weakened EAWM winds and thereby the intensified upper water stratification. The shifts in thaumarchaeal community were in parallel with variation of $\delta^{15}N_{org}$, with more shallow-*Thaumarchaeota* matching with lower $\delta^{15}N_{org}$ values, suggesting a close positive coupling of eutrophic zone AO and NF. The coupling relationship is potentially associated with consumption of dissolved O_2 in subsurface waters by AO and related processes that are modulated by water stratification and wind strength of the EAWM.

Acknowledgements

We appreciate the help of the crew onboard the R/V Marion Dufresne during a WEPAMA cruise of International Marine Past Global Change Study (IMAGES) program in 2001 and during the MD147-Marco-Polo Cruise in 2005. We thank Enqing Huang for providing the planktonic oxygen isotope data of MD05-2897. This work was supported by the State Key R&D project (grant No. 2016YFA0601104) and the National Natural Science Foundation of China (grant No. 41606047). Yige Zhang and one anonymous reviewer are thanked for their constructive comments.

References

Altabet, M.A., Francois, R., Murray, D.W., Prell, W.L., 1995. Climate-related variations in denitrification in the Arabian sea from sediment $^{15}N/^{14}N$ ratios. Nature 373, 506–509.
Altabet, M.A., Pilskaln, C., Thunell, R., Pride, C., Sigman, D., Chavez, F., Francois, R., 1999. The nitrogen isotope biogeochemistry of sinking particles from the margin of the eastern North Pacific. Deep-Sea Res., Part 1 46, 655–679.
Basse, A., Zhu, C., Versteegh, G.J., Fischer, G., Hinrichs, K.U., Mollenhauer, G., 2014. Distribution of intact and core tetraether lipids in water column profiles of suspended particulate matter off Cape Blanc, NW Africa. Org. Geochem. 72, 1–13.
Beman, J.M., Popp, B.N., Francis, C.A., 2008. Molecular and biogeochemical evidence for ammonia oxidation by marine Crenarchaeota in the Gulf of California. ISME J. 2, 429–441.
Beman, J.M., Popp, B.N., Alford, S.E., 2012. Quantification of ammonia oxidation rates and ammonia-oxidizing archaea and bacteria at high resolution in the Gulf of California and eastern tropical North Pacific Ocean. Limnol. Oceanogr. 57, 711–726.
Benavides, M., Voss, M., 2015. Five decades of N_2 fixation research in the North Atlantic Ocean. Front. Mar. Sci. 2, 40.
Berges, J.A., Mulholland, M.R., 2008. Enzymes and nitrogen cycling. In: Capone, D., Bronk, D., Mulholland, M., Carpenter, E. (Eds.), Nitrogen in the Marine Environment, 2nd edition. Elsevier Inc, pp. 1385–1444.
Boyce, D.G., Lewis, M.R., Worm, B., 2010. Global phytoplankton decline over the past century. Nature 466, 591–596.
Brandes, J.A., Devol, A.H., Yoshinari, T., Jayakumar, D.A., Naqvi, S.W.A., 1998. Isotopic composition of nitrate in the central Arabian Sea and eastern tropical North Pacific: a tracer for mixing and nitrogen cycles. Limnol. Oceanogr. 43, 1680–1689.
Broecker, W.S., Henderson, G.M., 1998. The sequence of events surrounding Termination II and their implications for the cause of glacial–interglacial CO_2 changes. Paleoceanography 13, 352–364.
Canfield, D.E., Glazer, A.N., Falkowski, P.G., 2010. The evolution and future of Earth's nitrogen cycle. Science 330, 192–196.
Church, M.J., Mahaffey, C., Letelier, R.M., Lukas, R., Zehr, J.P., Karl, D.M., 2009. Physical forcing of nitrogen fixation and diazotroph community structure in the North Pacific subtropical gyre. Glob. Biogeochem. Cycles 23, GB2020.
Church, M.J., Wai, B.R.K., Karl, D.M., DeLong, E.F., 2010. Abundances of crenarchaeal amoA genes and transcripts in the Pacific Ocean. Environ. Microbiol. 12, 679–688.
Cline, J., Kaplan, I., 1975. Isotopic fractionation of dissolved nitrate during denitrification in the eastern tropical North Pacific Ocean. Mar. Chem. 3, 271–299.
Codispoti, L.A., Brandes, J.A., Christensen, J.P., Devol, A.H., Naqvi, S.W.A., Paerl, H.W., Yoshinari, T., 2001. The oceanic fixed nitrogen and nitrous oxide budgets: moving targets as we enter the anthropocene? Sci. Mar. 65, 85–105.
Cohen, Y., Gordon, L.I., 1979. Nitrous-oxide production in the ocean. J. Geophys. Res., Atmos. 84, 347–353.
DeLong, E.F., 1992. Archaea in coastal marine environments. Proc. Natl. Acad. Sci. USA 89, 5685–5689.
Deutsch, C., Sarmiento, J.L., Sigman, D.M., Gruber, N., Dunne, J.P., 2007. Spatial coupling of nitrogen inputs and losses in the ocean. Nature 445 (7124), 163.
Dittmar, T., Koch, B., Hertkorn, N., Kattner, G., 2008. A simple and efficient method for the solid-phase extraction of dissolved organic matter (SPE-DOM) from seawater. Limnol. Oceanogr., Methods 6, 230–235.
Dong, L., Li, L., Li, Q., Wang, H., Zhang, C.L., 2015. Hydroclimate implications of thermocline variability in the southern South China Sea over the past 180,000 yr. Quat. Res. 83, 370–377.
Du, C., Liu, Z., Kao, S.-J., Dai, M., 2017. Diapycnal fluxes of nutrients in an oligotrophic oceanic regime: the South China Sea. Geophys. Res. Lett. 44, 11510–11518.
Eppley, R.W., Peterson, B.J., 1979. Particulate organic matter flux and planktonic new production in the deep ocean. Nature 282, 677.
Falkowski, P.G., 1997. Evolution of the nitrogen cycle and its influence on the biological sequestration of CO_2 in the ocean. Nature 387, 272–275.
Francis, C.A., Beman, J.M., Kuypers, M.M., 2007. New processes and players in the nitrogen cycle: the microbial ecology of anaerobic and archaeal ammonia oxidation. ISME J. 1, 19–27.
Fuhrman, J.A., Davis, A.A., 1997. Widespread archaea and novel bacteria from the deep sea as shown by 16S rRNA gene sequences. Mar. Ecol. Prog. Ser. 150, 275–285.
Fuhrman, J.A., McCallum, K., Davis, A.A., 1992. Novel major archaebacterial group from marine plankton. Nature 356, 148–149.

Galand, P.E., Casamayor, E.O., Kirchman, D.L., Potvin, M., Lovejoy, C., 2009. Unique archaeal assemblages in the Arctic Ocean unveiled by massively parallel tag sequencing. ISME J. 3, 860–869.

Ganeshram, R.S., Pedersen, T.F., Calvert, S.E., Murray, J.W., 1995. Large changes in oceanic nutrient inventories from glacial to interglacial periods. Nature 376, 755–758.

Herfort, L., Schouten, S., Abbas, B., Veldhuis, M.J., Coolen, M.J., Wuchter, C., Boon, J.P., Herndl, G.J., Sinninghe Damsté, J.S., 2007. Variations in spatial and temporal distribution of Archaea in the North Sea in relation to environmental variables. Microb. Ecol. 62, 242–257.

Hernández-Sánchez, M., Woodward, E., Taylor, K., Henderson, G., Pancost, R., 2014. Variations in GDGT distributions through the water column in the South East Atlantic Ocean. Geochim. Cosmochim. Acta 132, 337–348.

Herndl, G.J., Reinthaler, T., Teira, E., van Aken, H., Veth, C., Pernthaler, A., Pernthaler, J., 2005. Contribution of Archaea to total prokaryotic production in the deep Atlantic Ocean. Appl. Environ. Microbiol. 71, 2303–2309.

Higginson, M.J., Maxwell, J.R., Altabet, M.A., 2003. Nitrogen isotope and chlorin paleoproductivity records from the Northern South China Sea: remote vs. local forcing of millennial- and orbital-scale variability. Mar. Geol. 201, 223–250.

Ho, S.L., Laepple, T., 2016. Flat meridional temperature gradient in the early Eocene in the subsurface rather than surface ocean. Nat. Geosci. 9, 606.

Horikawa, K., Minagawa, M., Kato, Y., Murayama, M., Nagao, S., 2006. N_2 fixation variability in the oligotrophic Sulu Sea, western equatorial Pacific region over the past 83 kyr. J. Oceanogr. 62, 427–439.

Hu, A., Jiao, N., Zhang, C.L., 2011. Community structure and function of planktonic crenarchaeota: changes with depth in the South China Sea. Microb. Ecol. 62, 549–563.

Huang, E., Tian, J., 2012. Sea-level rises at Heinrich stadials of early Marine Isotope Stage 3: evidence of terrigenous *n*-alkane input in the southern South China Sea. Glob. Planet. Change 94, 1–12.

Jia, G., Li, Z., 2011. Easterly denitrification signal and nitrogen fixation feedback documented in the western Pacific sediments. Geophys. Res. Lett. 38, L24605.

Jia, G., Wang, X., Guo, W., Dong, L., 2017. Seasonal distribution of archaeal lipids in surface water and its constraint on their sources and the TEX_{86} temperature proxy in sediments of the South China Sea. J. Geophys. Res. https://doi.org/10.1002/2016JG003732.

Jia, G., Zhang, J., Chen, J., Peng, P.A., Zhang, C.L., 2012. Archaeal tetraether lipids record subsurface water temperature in the South China Sea. Org. Geochem. 50, 68–77.

Kao, S.J., Liu, K.K., Hsu, S.C., Chang, Y.P., Dai, M.H., 2008. North Pacific-wide spreading of isotopically heavy nitrogen during the last deglaciation: evidence from the western Pacific. Biogeosciences 5, 1641–1650.

Karner, M.B., DeLong, E.F., Karl, D.M., 2001. Archaeal dominance in the mesopelagic zone of the Pacific Ocean. Nature 409, 507–510.

Kienast, M., 2000. Unchanged nitrogen isotopic composition of organic matter in the South China Sea during the last climatic cycle: global implications. Paleoceanography 15, 244–253.

Kienast, M., Calvert, S.E., Pelejero, C., Grimalt, J.O., 2001. A critical review of marine sedimentary $\delta^{13}C_{org}$–pCO_2 estimates: new palaeorecords from the South China Sea and a revisit of other low-latitude $\delta^{13}C_{org}$–pCO_2 records. Glob. Biogeochem. Cycles 15, 113–127.

Kienast, M., Higginson, M.J., Mollenhauer, G., Eglinton, T.I., Chen, M.T., Calvert, S.E., 2005. On the sedimentological origin of down-core variations of bulk sedimentary nitrogen isotope ratios. Paleoceanography 20, PA2009.

Kim, J.-H., Schouten, S., Rodrigo-Gamiz, M., Rampen, S., Marino, G., Huguet, C., Helmke, P., Buscail, R., Hopmans, E.C., Pross, J., Sangiorgi, F., Middelburg, J.B.M., Sinninghe Damsté, J.S., 2015. Influence of deep-water derived isoprenoid tetraether lipids on the TEX_H^{86} paleothermometer in the Mediterranean Sea. Geochim. Cosmochim. Acta 150, 125–141.

Kim, J.H., Van der Meer, J., Schouten, S., Helmke, P., Willmott, V., Sangiorgi, F., Koç, N., Hopmans, E.C., Sinninghe Damsté, J.S., 2010. New indices and calibrations derived from the distribution of crenarchaeal isoprenoid tetraether lipids: implications for past sea surface temperature reconstructions. Geochim. Cosmochim. Acta 74 (16), 4639–4654.

Kim, J.-H., Villanueva, L., Zell, C., Sinninghe Damsté, J.S., 2016. Biological source and provenance of deep-water derived isoprenoid tetraether lipids along the Portuguese continental margin. Geochim. Cosmochim. Acta 172, 177–204.

Koops, H.P., Pommerening-Roser, A., 2001. Distribution and ecophysiology of the nitrifying bacteria emphasizing cultured species. FEMS Microbiol. Ecol. 37, 1–9.

Kuypers, M.M., van Breugel, Y., Schouten, S., Erba, E.J., Sinninghe Damsté, J.S., 2004. N_2-fixing cyanobacteria supplied nutrient N for Cretaceous oceanic anoxic events. Geology 32, 853–856.

Li, Q., Zheng, F., Chen, M., Xiang, R., Qiao, P., Shao, L., Cheng, X., 2010. Glacial paleoceanography off the mouth of the Mekong River, southern South China Sea, during the last 500 ka. Quat. Res. 73, 563–572.

Li, Z., Jia, G., 2011. Separation of total nitrogen from sediments into organic and inorganic forms for isotopic analysis. Org. Geochem. 42, 296–299.

Lincoln, S.A., Wai, B., Eppley, J.M., Church, M.J., Summons, R.E., DeLong, E.F., 2014. Planktonic Euryarchaeota are a significant source of archaeal tetraether lipids in the ocean. Proc. Natl. Acad. Sci. USA 111, 9858–9863.

Lisiecki, L.E., Raymo, M.E., 2005. A Pliocene–Pleistocene stack of 57 globally distributed benthic $\delta^{18}O$ records. Paleoceanography 20 (1).

Liu, K.-K., Su, M.-J., Hsueh, C.-R., Gong, G.-C., 1996. The nitrogen isotopic composition of nitrate in the Kuroshio Water northeast of Taiwan: evidence for nitrogen fixation as a source of isotopically light nitrate. Mar. Chem. 54, 273–292.

Liu, Q., Tolar, B.B., Ross, M.J., Cheek, J.B., Sweeney, C.M., Wallsgrove, N.J., Popp, B.N., Hollibaugh, J.T., 2018. Light and temperature control the seasonal distribution of thaumarchaeota in the South Atlantic bight. ISME J. 12, 1473–1485.

Luo, Y.-W., Lima, I.D., Karl, D.M., Deutsch, C.A., Doney, S.C., 2014. Data-based assessment of environmental controls on global marine nitrogen fixation. Biogeosciences 11, 691–708.

Massana, R., DeLong, E.F., Pedros-Alio, C., 2000. A few cosmopolitan phylotypes dominate planktonic archaeal assemblages in widely different oceanic provinces. Appl. Environ. Microbiol. 66, 1777–1787.

Meckler, A.N., Ren, H., Sigman, D.M., Gruber, N., Plessen, B., Schubert, C.J., Haug, G.H., 2011. Deglacial nitrogen isotope changes in the Gulf of Mexico: evidence from bulk sedimentary and foraminifera-bound nitrogen in Orca Basin sediments. Paleoceanography 26, PA4216.

Mincer, T.J., Church, M.J., Taylor, L.T., Preston, C., Karl, D.M., DeLong, E.F., 2007. Quantitative distribution of presumptive archaeal and bacterial nitrifiers in Monterey Bay and the North Pacific Subtropical Gyre. Environ. Microbiol. 9, 1162–1175.

Mobius, J., Gaye, B., Lahajnar, N., Bahlmann, E., Emeis, K.C., 2011. Influence of diagenesis on sedimentary $\delta^{15}N$ in the Arabian Sea over the last 130 kyr. Mar. Geol. 284, 127–138.

Moore, C.M., Mills, M.M., Achterberg, E.P., Geider, R.J., LaRoche, J., Lucas, M.I., McDonagh, E.L., Pan, X., Poulton, A.J., Rijkenberg, M.J.A., Suggett, D.J., Ussher, S.J., Woodward, E.M.S., 2009. Large-scale distribution of Atlantic nitrogen fixation controlled by iron availability. Nat. Geosci. 2, 867–871.

Murray, A., Preston, C., Massana, R., Taylor, L., Blakis, A., Wu, K., DeLong, E., 1998. Seasonal and spatial variability of bacterial and archaeal assemblages in the coastal waters near Anvers Island, Antarctica. Appl. Environ. Microbiol. 64, 2585–2595.

Naqvi, S.W.A., 1991. N_2O production in the ocean. Nature 349, 373–374.

Pearson, A., Pi, Y., Zhao, Y., Li, W.-J., Li, Y., Inskeep, W., Perevelova, A., Romanek, C., Li, S., Zhang, C.L., 2008. Factors controlling the distribution of archaeal tetraethers in terrestrial hot springs. Appl. Environ. Microbiol. 74, 3523–3532.

Peng, X., Fuchsman, C.A., Jayakumar, A., Oleynik, S., Martens-Habbena, W., Devol, A.H., Ward, B.B., 2015. Ammonia and nitrite oxidation in the Eastern Tropical North Pacific. Glob. Biogeochem. Cycles 29, 2034–2049.

Polovina, J.J., Howell, E.A., Abecassis, M., 2008. Ocean's least productive waters are expanding. Geophys. Res. Lett. 35, 1–5.

Qin, W., Amin, S.A., Martens-Habbena, W., Walker, C.B., Urakawa, H., Devol, A.H., et al., 2014. Marine ammonia-oxidizing archaeal isolates display obligate mixotrophy and wide ecotypic variation. Proc. Natl. Acad. Sci. USA 111, 12504–12509.

Ren, H., Sigman, D., Meckler, A., Plessen, B., Robinson, R., Rosenthal, Y., Haug, G., 2009. Foraminiferal isotope evidence of reduced nitrogen fixation in the ice age Atlantic Ocean. Science 323, 244–248.

Ren, H., Sigman, D.M., Chen, M.T., Kao, S.J., 2012. Elevated foraminifera-bound nitrogen isotopic composition during the last ice age in the South China Sea and its global and regional implications. Glob. Biogeochem. Cycles 26, GB1031.

Ren, H., Sigman, D.M., Martínez-García, A., Anderson, R.F., Chen, M.-T., Ravelo, A.C., Straub, M., Wong, G.T.F., Haug, G.H., 2017. Impact of glacial/interglacial sea level change on the ocean nitrogen cycle. Proc. Natl. Acad. Sci. USA 114, E6759–E6766.

Rush, D., Sinninghe Damsté, J.S., 2017. Lipids as paleomarkers to constrain the marine nitrogen cycle. Environ. Microbiol. 19 (6), 2119–2132.

Santoro, A.E., Buchwald, C., McIlvin, M.R., Casciotti, K.L., 2011. Isotopic signature of N_2O produced by marine ammonia-oxidizing archaea. Science 333, 1282–1285.

Schaefer, S.C., Hollibaugh, J.T., 2017. Temperature decouples ammonium and nitrite oxidation in coastal waters. Environ. Sci. Technol. 51, 3157–3164.

Schouten, S., Hopmans, E.C., Schefuß, E., Sinninghe Damsté, J.S., 2002. Distributional variations in marine crenarchaeotal membrane lipids: a new tool for reconstructing ancient sea water temperatures? Earth Planet. Sci. Lett. 204, 265–274.

Schouten, S., van der Meer, M.J.T., Hopmans, E.C., Sinninghe Damsté, J.S., 2007. Archaeal and bacterial glycerol dialkyl glycerol tetraether lipids in hot springs of Yellowstone National Park. Appl. Environ. Microbiol. 73, 6181–6191.

Schouten, S., Pitcher, A., Hopmans, E.C., Villanueva, L., van Bleijswijk, J., Sinninghe Damsté, J.S., 2012. Intact polar and core glycerol dibiphytanyl glycerol tetraether lipids in the Arabian Sea oxygen minimum zone, I: selective preservation and degradation in the water column and consequences for the TEX_{86}. Geochim. Cosmochim. Acta 98, 228–243.

Shimada, H., Nimoto, N., Shida, Y., Oshima, T., Yamagishi, A., 2002. Complete polar lipid composition of *Thermoplasma acidophilum* HO-62 determined by high-performance liquid chromatography with evaporative light-scattering detection. J. Bacteriol. 184, 556–563.

Shiozaki, T., Ijichi, M., Isobe, K., Hashihama, F., Nakamura, K., Ehama, M., Hayashizaki, K., Takahashi, K., Hamasaki, K., Furuya, K., 2016. Nitrification and its influence on biogeochemical cycles from the equatorial Pacific to the Arctic Ocean. ISME J. 10, 2184–2197.

Sinninghe Damsté, J.S., Schouten, S., Hopmans, E.C., van Duin, A.C.T., Geenevasen, J.A.J., 2002. Crenarchaeol: the characteristic core glycerol dibiphytanyl glycerol tetraether membrane lipid of cosmopolitan pelagic crenarchaeota. J. Lipid Res. 43, 1641–1651.

Sintes, E., Bergauer, K., De Corte, D., Yokokawa, T., Herndl, G.J., 2013. Archaeal amoA gene diversity points to distinct biogeography of ammonia-oxidizing Crenarchaeota in the ocean. Environ. Microbiol. 15, 1647–1658.

Smith, J.M., Casciotti, K.L., Chavez, F.P., Francis, C.A., 2014. Differential contributions of archaeal ammonia oxidizer ecotypes to nitrification in coastal surface waters. ISME J. 8, 1704–1714.

Sowers, T., Alley, R.B., Jubenville, J., 2003. Ice core records of atmospheric N_2O covering the last 106,000 years. Science 301, 945–948.

Spang, A., Hatzenpichler, R., Brochier-Armanet, C., Rattei, T., Tischler, P., Spieck, E., Streit, W., Stahl, D.A., Wagner, M., Schleper, C., 2010. Distinct gene set in two different lineages of ammonia-oxidizing archaea supports the phylum Thaumarchaeota. Trends Microbiol. 18, 331–340.

Stahl, D.A., de la Torre, J.R., 2012. Physiology and diversity of ammonia-oxidizing archaea. In: Gottesman, S., Harwood, C.S., Schneewind, O. (Eds.), Annu. Rev. Microbiol., vol. 66, pp. 83–101.

Stramma, L., Johnson, G.C., Sprintall, J., Mohrholz, V., 2008. Expanding oxygen-minimum zones in the tropical oceans. Science 320, 655–658.

Straub, M., Sigman, D.M., Ren, H., Martinez-Garcia, A., Meckler, A.N., Hain, M.P., Haug, G.H., 2013. Changes in North Atlantic nitrogen fixation controlled by ocean circulation. Nature 501, 200–204.

Su, X., Liu, C., Beaufort, L., Tian, J., Huang, E., 2013. Late Quaternary coccolith records in the South China Sea and East Asian monsoon dynamics. Glob. Planet. Change 111, 88–96.

Su, X., Liu, C., Beaufort, L., Barbarin, N., Jian, Z., 2015. Differences in Late Quaternary primary productivity between the western tropical Pacific and the South China Sea: evidence from coccoliths. Deep-Sea Res., Part 2, Top. Stud. Oceanogr. 122, 131–141.

Taylor, K.W., Huber, M., Hollis, C.J., Hernandez-Sanchez, M.T., Pancost, R.D., 2013. Re-evaluating modern and Palaeogene GDGT distributions: implications for SST reconstructions. Glob. Planet. Change 108, 158–174.

Tian, J., Wang, P., Cheng, X., 2004. Responses of foraminiferal isotopic variations at ODP Site 1143 in the southern South China Sea to orbital forcing. Sci. China Ser. D, Earth Sci. 47 (10), 943–953.

Tierney, J.E., Tingley, M.P., 2015. A TEX_{86} surface sediment database and extended Bayesian calibration. Sci. Data 2, 150029.

Tolar, B.B., King, G.M., Hollibaugh, J.T., 2013. An analysis of Thaumarchaeota populations from the Northern Gulf of Mexico. Front. Microbiol. 4, 72. https://doi.org/10.3389/fmicb.2013.00072.

Tseng, C.-H., Chiang, P.-W., Lai, H.-C., Shiah, F.-K., Hsu, T.-C., Chen, Y.-L., Wen, L.-S., Tseng, C.-M., Shieh, W.-Y., Saeed, I., Halgamuge, S., Tang, S.-L., 2015. Prokaryotic assemblages and metagenomes in pelagic zones of the South China Sea. BMC Genomics 16.

Turich, C., Freeman, K.H., Bruns, M.A., Conte, M., Jones, A.D., Wakeham, S.G., 2007. Lipids of marine Archaea: patterns and provenance in the water-column and sediments. Geochim. Cosmochim. Acta 71, 3272–3291.

Urakawa, H., Martens-Habbena, W., Huguet, C., de la Torre, J.R., Ingalls, A.E., Devol, A.H., et al., 2014. Ammonia availability shapes the seasonal distribution and activity of archaeal and bacterial ammonia oxidizers in the Puget Sound Estuary. Limnol. Oceanogr. 59, 1321–1335.

Villanueva, L., Schouten, S., Damste, J.S.S., 2015. Depth-related distribution of a key gene of the tetraether lipid biosynthetic pathway in marine Thaumarchaeota. Environ. Microbiol. 17, 3527–3539.

Wada, E., Hattori, A., 1976. Natural abundance of ^{15}N in particulate organic matter in the North Pacific Ocean. Geochim. Cosmochim. Acta 40, 249–251.

Wang, Y., Cheng, H., Edwards, R.L., Kong, X., Shao, X., Chen, S., Wu, J., Jiang, X., Wang, X., An, Z., 2008. Millennial- and orbital-scale changes in the East Asian monsoon over the past 224,000 years. Nature 451 (7182), 1090.

Wong, G.T.F., Chung, S.-W., Shiah, F.-K., Chen, C.-C., Wen, L.-S., Liu, K.-K., 2002. Nitrate anomaly in the upper nutricline in the northern South China Sea—evidence for nitrogen fixation. Geophys. Res. Lett. 29. 2097.

Wong, G.T.F., Ku, T.-L., Mulholland, M., Tseng, C.-M., Wang, D.-P., 2007. The South East Asian Time-series Study (SEATS) and the biogeochemistry of the South China Sea—an overview. Deep-Sea Res., Part 2 54, 1434–1447.

Wu, J., Chung, S.-W., Wen, L.-S., Liu, K.-K., Chen, Y.-L.L., Chen, H.-Y., Karl, D.M., 2003. Dissolved inorganic phosphorus, dissolved iron, and Trichodesmium in the oligotrophic South China Sea. Glob. Biogeochem. Cycles 17, 1008.

Wuchter, C., Schouten, S., Coolen, M.J.L., Sinninghe Damsté, J.S., 2004. Temperature dependent variation in the distribution of tetraether membrane lipids of marine Crenarchaeota: implications for TEX_{86} paleothermometry. Paleoceanography 19, PA4028.

Wuchter, C., Schouten, S., Wakeham, S.G., Sinninghe Damsté, J.S., 2005. Temporal and spatial variation in tetraether membrane lipids of marine Crenarchaeota in particulate organic matter: implications for TEX86 paleothermometry. Paleoceanography 20, PA3013.

Wuchter, C., Abbas, B., Coolen, M.J.L., Herfort, L., van Bleijswijk, J., Timmers, P., Strous, M., Teira, E., Herndl, G.J., Middelburg, J.J., Schouten, S., Damste, J.S.S., 2006. Archaeal nitrification in the ocean. Proc. Natl. Acad. Sci. USA 103, 12317–12322.

Xia, X., Guo, W., Liu, H., 2015. Dynamics of the bacterial and archaeal communities in the Northern South China Sea revealed by 454 pyrosequencing of the 16S rRNA gene. Deep-Sea Res., Part 2 117, 97–107.

Xie, S., 2018. The shift of biogeochemical cycles indicative of the progressive marine ecosystem collapse across the Permian–Triassic boundary: an analog to modern oceans. Sci. China Earth Sci. 61, 1379–1383.

Yamamoto, M., Sai, H., Chen, M.T., Zhao, M., 2013. The East Asian winter monsoon variability in response to precession during the past 150 000 yr. Clim. Past 9, 2777–2788.

Yool, A., Martin, A.P., Ferandez, C., Clark, D.R., 2007. The significance of nitrification for oceanic new production. Nature 447, 999–1002.

Zehr, J.P., Kudela, R.M., 2011. Nitrogen cycle of the open ocean: from genes to ecosystems. Annu. Rev. Mar. Sci. 3, 197–225.

Zhang, C.L., Xie, W., Martin-Cuadrado, A.-B., Rodriguez-Valera, F., 2015. Marine Group II Archaea, potentially important players in the global ocean carbon cycle. Front. Microbiol. 6, 1108.

Zhang, Y.G., Liu, X., 2018. Export depth of the TEX_{86} signal. Paleoceanogr. Paleoclimatol. 7, 666–671.